

Cavity Bounds on Higher-Order Lorentz-Violating Coefficients

Stephen R. Parker,¹ Matthew Mewes,² Paul L. Stanwix,¹ and Michael E. Tobar¹

¹*School of Physics, The University of Western Australia, Crawley WA 6009, Australia*

²*Department of Physics and Astronomy, Swarthmore College, Swarthmore, Pennsylvania 19081, USA*

(Dated: March 20, 2022)

We determine the sensitivity of a modern Michelson-Morley resonant-cavity experiment to higher-order nonbirefringent and nondispersive coefficients of the Lorentz-violating Standard-Model Extension. Data from a recent year-long run of the experiment is used to place the first experimental bounds on coefficients associated with nonrenormalizable Lorentz-violating operators.

Over the past century, the behavior of light has been scrutinized for possible defects in Einstein's theory of special relativity. Recent advances in theory and experiment have led to renewed interest and a large number of tests of Lorentz invariance, the symmetry behind relativity [1]. These studies are motivated, in part, by the possibility that theories incorporating quantum gravity may lead to small violations of Lorentz invariance at low energies, providing an avenue for searches for fundamental physics [2]. New work has uncovered a very large class of unexplored higher-order violations in photons [3]. This letter provides the first laboratory-based constraints on these violations, initiating a new class of tests of Lorentz invariance.

A wide variety of experimental techniques have been employed in searches for Lorentz violation [1]. One particularly sensitive type of experiment is based on electromagnetic resonant cavities [4–8]. These are considered descendants of the classic Michelson-Morley experiment [9] and are analyzed using a theoretical framework known as the Standard-Model Extension (SME) [10, 11]. While the SME describes general violations of Lorentz invariance in any system, most studies have focused on the minimal SME, which restricts attention to operators of renormalizable dimension in flat spacetime. However, the photon sector of the SME has recently been extended to include operators of arbitrary dimension [3]. Here we search for the effects of these higher-order nonrenormalizable violations using the cavity-based experiment described in [4].

The photon sector of the nonminimal SME contains a large number of possible violations that lead to different unconventional phenomena. It is convenient to split these violations into subclasses based on their physical effects. Two subclasses that are particularly useful are based on cosmological birefringence and dispersion. These unconventional features affect the way light propagates through empty space and can be tested with extreme precision using astrophysical sources [12–14]. Violations that do not cause birefringence or dispersion are not easily detected in astrophysical observations. However, they can often be measured in laboratory-based experiments, which complement astrophysical tests.

In the SME, the higher-order nonbirefringent nondis-

persive violations are controlled by a set of coefficients that are denoted by $(\bar{c}_F^{(d)})_{njm}^{(0E)}$. These are referred to as camouflage coefficients, due to their benign nature, and are the primary focus of this work. The d index on the coefficients is the dimension of the associated operator and only takes on even values $d \geq 6$. It should be noted that there are nonbirefringent nondispersive violations among the renormalizable $d = 4$ operators. The coefficients associated with these operators are $c_{(I)jm}^{(4)}$ and were the main focus of previous cavity experiments [4–8]. We will include the renormalizable coefficients in our analysis for completeness. We will restrict our analysis of nonrenormalizable violations to the two lowest-order cases, $d = 6, 8$, for simplicity. However, the techniques outlined here could be applied to higher-order violations.

The Lorentz violations associated with the $c_{(I)jm}^{(4)}$ and the $(\bar{c}_F^{(d)})_{njm}^{(0E)}$ coefficients lead to tiny shifts in the resonant frequencies of cavities. As described in Ref. [3], the frequency shift resulting from coefficients of a given dimension takes the generic form

$$\frac{\delta\nu}{\nu} = \sum_{njm} \mathcal{M}_{njm}^{\text{cav}} c_{njm}^{\text{cav}}, \quad (1)$$

to first order in coefficients for Lorentz violation. The index n characterizes the frequency/wavelength dependence of the coefficient, but is irrelevant for dimension $d = 4$. The jm indices represent the usual angular-momentum quantum numbers, which characterize the rotational properties of the coefficients. Note that a violation of rotation invariance serves as our signal of Lorentz violation.

The $\mathcal{M}_{njm}^{\text{cav}}$ are experiment-dependent constants that determine the sensitivity to each coefficient and are calculated using the conventional solutions to the Maxwell equations in the cavity. The “cav” designation indicates a reference frame fixed to the cavity with the z direction along the symmetry axis. This frame is not inertial, so the c_{njm}^{cav} coefficients change as the cavity rotates. We need to express the frequency in terms of fixed coefficients in an inertial frame, which by convention is taken as a Sun-centered celestial equatorial frame [1]. Ignoring boosts, the transformation is achieved by a series of rotations that, in the current language, take

the form of Wigner matrices. The result can be written $\delta\nu/\nu = \sum_{mm'} A_{mm'} e^{im\phi + im'\omega_{\oplus}T}$, where

$$A_{mm'} = \sum_{nj} \mathcal{M}_{njm'}^{\text{cav}} d_{m'm}^{(j)}(-\frac{\pi}{2}) d_{mm'}^{(j)}(-\chi) c_{njm'}^{\text{Sun}}. \quad (2)$$

In these expressions, $d_{mm'}^{(j)}$ are the ‘‘little’’ Wigner matrices, χ is the colatitude of the laboratory, $\omega_{\oplus}T$ is the right ascension of the laboratory, and ϕ is the angle between south and the cavity symmetry axis. The $c_{njm'}^{\text{Sun}}$ are constant Sun-frame coefficients. Here we assume the cavity lies in the horizontal plane. The $A_{mm'}$ amplitudes obey the relation $A_{mm'}^* = A_{(-m)(-m')}$. This implies that the frequency shift is real, as expected.

The experiment involves monitoring the beat frequency between resonances of two identical horizontal rotating cavities. Violations of rotation symmetry can introduce orientation dependence. This would manifest as a dependence on the orientation with respect to the laboratory (ϕ) or in variations at the sidereal frequency $\omega_{\oplus} \simeq 2\pi/(23 \text{ hr } 56 \text{ min})$ as the laboratory rotates throughout the day. Since the cavities of interest are perpendicular, we let one cavity lie at an angle ϕ and the other at an angle $\phi + \pi/2$. This leads to $\nu_{\text{beat}}/\nu = \sum A_{mm'}^{\text{beat}} e^{im\phi + im'\omega_{\oplus}T}$, where

$$A_{mm'}^{\text{beat}} = (1 - i^m) A_{mm'}. \quad (3)$$

The beat amplitudes $A_{mm'}^{\text{beat}}$ obey the same conjugation relationship as the $A_{mm'}$ amplitudes.

It is convenient to express the beat frequency in terms of sines and cosines with real amplitudes. Trigonometric expansions can then be used to mix together frequency sidebands of the same multiple of sidereal frequency, m' , which has the benefit of combining the positive and negative m and m' terms allowing the data to be fit to all components. This gives

$$\frac{\nu_{\text{beat}}}{\nu} = \sum_{m \geq 0} [C_m(T) \cos(m\phi) + S_m(T) \sin(m\phi)], \quad (4)$$

where $C_m(T)$ and $S_m(T)$ are amplitudes that vary slowly, at integer multiples of the sidereal frequency. They are given by

$$\begin{aligned} C_m(T) &= \sum_{m' \geq 0} [C_{mm'}^C \cos(m'\omega_{\oplus}T) + C_{mm'}^S \sin(m'\omega_{\oplus}T)], \\ S_m(T) &= \sum_{m' \geq 0} [S_{mm'}^C \cos(m'\omega_{\oplus}T) + S_{mm'}^S \sin(m'\omega_{\oplus}T)], \end{aligned} \quad (5)$$

with

$$\begin{aligned} C_{mm'}^C &= 2\eta_m \eta_{m'} \text{Re}[A_{mm'}^{\text{beat}} + A_{m(-m')}^{\text{beat}}], \\ C_{mm'}^S &= -2\eta_m \text{Im}[A_{mm'}^{\text{beat}} - A_{m(-m')}^{\text{beat}}], \\ S_{mm'}^C &= -2\eta_{m'} \text{Im}[A_{mm'}^{\text{beat}} + A_{m(-m')}^{\text{beat}}], \\ S_{mm'}^S &= -2\text{Re}[A_{mm'}^{\text{beat}} - A_{m(-m')}^{\text{beat}}], \end{aligned} \quad (6)$$

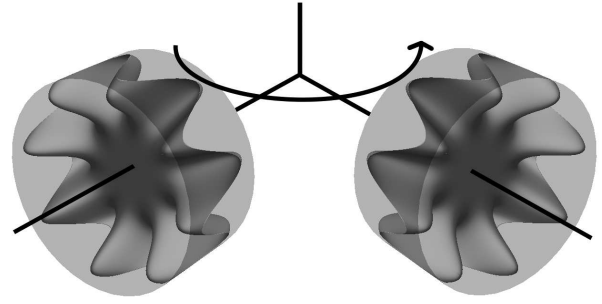


FIG. 1: Diagram of the sapphire orientation. The wave patterns represent the dominate axial field in the $\text{WGH}_{8,0,0}$ mode. In this experiment, the sapphire radius and height are approximately 1.5 cm and 3 cm, respectively. The oscillator pair is rotated about the vertical axis.

where, for convenience, we define $\eta_0 = 1/2$ and $\eta_m = 1$ when $m \neq 0$.

The data used in this analysis are from an experiment run at the University of Western Australia between 2004 and 2006 [4]. The experiment is based on two orthogonally aligned cryogenic sapphire oscillators lying in the horizontal plane and rotated around the vertical axis, as illustrated in Fig. 1. The resonators were excited at microwave frequencies to produce a standing-wave whispering-gallery mode with a dominant electric field in the axial direction and 8 azimuthal field variations (designated $\text{WGH}_{8,0,0}$). The beat frequency was recorded as a function of time and orientation. For a more detailed description of the experiment, see Ref. [4].

To calculate the $\mathcal{M}_{njm}^{\text{cav}}$ matrices needed in (2) the electric fields in the cavities must be modeled. Maxwell’s equations are solved to obtain analytic approximations for the fields inside and outside the sapphire [16]. For example, the dominate axial component of the field inside the sapphire crystal is reasonably described by

$$E_z \propto J_8(695 \text{ m}^{-1} \rho) \cos(8\phi) \cos(104 \text{ m}^{-1} z) \quad (7)$$

in cylindrical coordinates (ρ, ϕ, z) . The other field components are of a similar form. It is found that over 98% of the electric-field energy is confined within the actual sapphire crystal. Consequently, we neglect the contribution from the fields outside the sapphire. Using the fields inside the sapphire, we generate estimates for the $\mathcal{M}_{njm}^{\text{cav}}$ matrices via the methods outlined in Ref. [3]. We then use these to express the amplitudes in (6) in terms of the coefficients for Lorentz violation. The results are shown in Table I.

Similar to Ref. [5], the data is demodulated at twice the turntable rotation frequency (2ϕ) over a period of 500 rotations and fit to the amplitudes C_m and S_m in (4). The time derivative of the data is then weighted, to ensure that the power spectral density of the residuals is white, and fit to the appropriate frequencies of interest from (6).

dimension	m	m'	$C_{mm'}^C$	$C_{mm'}^S$	$S_{mm'}^C$	$S_{mm'}^S$
$d = 4$	2	0	$-0.27 c_{(I)20}^{(4)}$	0	0	0
	2	1	$0.27 \text{Re}(c_{(I)21}^{(4)})$	$-0.27 \text{Im}(c_{(I)21}^{(4)})$	$0.52 \text{Im}(c_{(I)21}^{(4)})$	$0.52 \text{Re}(c_{(I)21}^{(4)})$
	2	2	$-0.39 \text{Re}(c_{(I)22}^{(4)})$	$0.39 \text{Im}(c_{(I)22}^{(4)})$	$-0.32 \text{Im}(c_{(I)22}^{(4)})$	$-0.32 \text{Re}(c_{(I)22}^{(4)})$
$d = 6$	2	0	$-3.2 (\overline{c}_F^{(6)})_{220}^{(0E)}$	0	0	0
	2	1	$3.3 \text{Re}((\overline{c}_F^{(6)})_{221}^{(0E)})$	$-3.3 \text{Im}((\overline{c}_F^{(6)})_{221}^{(0E)})$	$6.2 \text{Im}((\overline{c}_F^{(6)})_{221}^{(0E)})$	$6.2 \text{Re}((\overline{c}_F^{(6)})_{221}^{(0E)})$
	2	2	$-4.7 \text{Re}((\overline{c}_F^{(6)})_{222}^{(0E)})$	$4.7 \text{Im}((\overline{c}_F^{(6)})_{222}^{(0E)})$	$-3.9 \text{Im}((\overline{c}_F^{(6)})_{222}^{(0E)})$	$-3.9 \text{Re}((\overline{c}_F^{(6)})_{222}^{(0E)})$
$d = 8$	2	0	$0.18 (\overline{c}_F^{(8)})_{220}^{(0E)}$ $-17 (\overline{c}_F^{(8)})_{420}^{(0E)}$ $-3.6 (\overline{c}_F^{(8)})_{440}^{(0E)}$	0	0	0
	2	1	$-0.19 \text{Re}((\overline{c}_F^{(8)})_{221}^{(0E)})$ $+18 \text{Re}((\overline{c}_F^{(8)})_{421}^{(0E)})$ $-8.6 \text{Re}((\overline{c}_F^{(8)})_{441}^{(0E)})$	$0.19 \text{Im}((\overline{c}_F^{(8)})_{221}^{(0E)})$ $-18 \text{Im}((\overline{c}_F^{(8)})_{421}^{(0E)})$ $+8.6 \text{Im}((\overline{c}_F^{(8)})_{441}^{(0E)})$	$-0.35 \text{Im}((\overline{c}_F^{(8)})_{221}^{(0E)})$ $+33 \text{Im}((\overline{c}_F^{(8)})_{421}^{(0E)})$ $+3.8 \text{Im}((\overline{c}_F^{(8)})_{441}^{(0E)})$	$-0.35 \text{Re}((\overline{c}_F^{(8)})_{221}^{(0E)})$ $+33 \text{Re}((\overline{c}_F^{(8)})_{421}^{(0E)})$ $+3.8 \text{Re}((\overline{c}_F^{(8)})_{441}^{(0E)})$
	2	2	$0.27 \text{Re}((\overline{c}_F^{(8)})_{222}^{(0E)})$ $-25 \text{Re}((\overline{c}_F^{(8)})_{422}^{(0E)})$ $+0.84 \text{Re}((\overline{c}_F^{(8)})_{442}^{(0E)})$	$-0.27 \text{Im}((\overline{c}_F^{(8)})_{222}^{(0E)})$ $+25 \text{Im}((\overline{c}_F^{(8)})_{422}^{(0E)})$ $-0.84 \text{Im}((\overline{c}_F^{(8)})_{442}^{(0E)})$	$0.22 \text{Im}((\overline{c}_F^{(8)})_{222}^{(0E)})$ $-21 \text{Im}((\overline{c}_F^{(8)})_{422}^{(0E)})$ $+11 \text{Im}((\overline{c}_F^{(8)})_{442}^{(0E)})$	$0.22 \text{Re}((\overline{c}_F^{(8)})_{222}^{(0E)})$ $-21 \text{Re}((\overline{c}_F^{(8)})_{422}^{(0E)})$ $+11 \text{Re}((\overline{c}_F^{(8)})_{442}^{(0E)})$
	2	3	$-3.1 \text{Re}((\overline{c}_F^{(8)})_{443}^{(0E)})$	$3.1 \text{Im}((\overline{c}_F^{(8)})_{443}^{(0E)})$	$1.8 \text{Im}((\overline{c}_F^{(8)})_{443}^{(0E)})$	$1.8 \text{Re}((\overline{c}_F^{(8)})_{443}^{(0E)})$
	2	4	$-8.1 \text{Re}((\overline{c}_F^{(8)})_{444}^{(0E)})$	$8.1 \text{Im}((\overline{c}_F^{(8)})_{444}^{(0E)})$	$-6.7 \text{Im}((\overline{c}_F^{(8)})_{444}^{(0E)})$	$-6.7 \text{Re}((\overline{c}_F^{(8)})_{444}^{(0E)})$

TABLE I: Nonzero sensitivities to coefficients for Lorentz violation for dimensions 4, 6, and 8. The numbers m and m' give the harmonics of the turntable rotation frequency and sidereal frequency, respectively. The dimension-6 amplitudes are in units of 10^{-26} GeV². The dimension-8 amplitudes are in units of 10^{-52} GeV⁴.

To place bounds on the coefficients for Lorentz violation, each dimension is considered to be independent of the others. For dimensions 4 and 6, we take combinations of the sine and cosine terms at each frequency to place constraints on the real and imaginary parts of $c_{(I)20}^{(4)}$, $c_{(I)21}^{(4)}$, $c_{(I)22}^{(4)}$, $(\overline{c}_F^{(6)})_{220}^{(0E)}$, $(\overline{c}_F^{(6)})_{221}^{(0E)}$, and $(\overline{c}_F^{(6)})_{222}^{(0E)}$. For dimension 8, the coefficients leading to variations at three ($m' = 3$) and four ($m' = 4$) times the sidereal frequency can be fully independently constrained. However, it is not possible to place individual bounds on the dimension-8 coefficients leading to variations at other frequencies ($m' = 0, 1, 2$). From Table I, we see that we are sensitive to one linear combination of three coefficients for $m' = 0$ and to four combinations of six real coefficients for $m' = 1$ and $m' = 2$. However, we can place constraints on the nine linear combinations. The results of our analysis are given in Table II. We note that several coefficients are significant at the 1σ level. However, all coefficients are consistent with zero at the 3σ level.

Our analysis focused on variations at twice the turntable frequency. Note that variations at four times the turntable frequency may also occur, in general. However, the $\pi/2$ separation of the resonators results in an identical shift in each cavity, and the sensitivities to coefficients at this frequency cancel out in the beat frequency. Using a different relative orientation or introducing a third resonator offset from the first two by $\pi/4$

would allow the coefficients $(\overline{c}_F^{(8)})_{440}^{(0E)}$, $(\overline{c}_F^{(8)})_{441}^{(0E)}$, and $(\overline{c}_F^{(8)})_{442}^{(0E)}$ to be bound independently. Different combinations of beat frequencies between the resonators could then be used to fully constrain the remaining coefficients.

In summary, we have placed constraints on dimension-6 and dimension-8 camouflage coefficients of the SME. These represent the first experimental measurements of nonrenormalizable Lorentz violation. We are able to measure five dimension-6 coefficients and thirteen combinations of dimension-8 coefficients. In our analysis, we found that the number of higher-dimension coefficients that can be accessed was restricted by the use of perpendicular cavities. Future experiments might achieve sensitivity to additional combinations of coefficients by orienting the cavities at other angles or by introducing a third cavity at an intermediate angle. Regardless, this work demonstrates the effectiveness of resonator experiments at detecting the higher-order Lorentz violation described by the nonminimal SME.

This work was supported by Australian Research Council Grant No. FL0992016.

[1] *Data Tables for Lorentz and CPT Violation*, V.A. Kostelecký and N. Russell, arXiv:0801.0287.

dimension	coefficient	measurement
$d = 4$	$c_{(I)20}^{(4)}$	$(3 \pm 16) \times 10^{-15}$
	$\text{Re}(c_{(I)21}^{(4)})$	$(20 \pm 23) \times 10^{-17}$
	$\text{Im}(c_{(I)21}^{(4)})$	$(137 \pm 71) \times 10^{-18}$
	$\text{Re}(c_{(I)22}^{(4)})$	$(-4 \pm 23) \times 10^{-17}$
	$\text{Im}(c_{(I)22}^{(4)})$	$(20 \pm 22) \times 10^{-18}$
$d = 6$	$(\bar{c}_F^{(6)})_{220}^{(0E)}$	$(3 \pm 13) \times 10^{10} \text{ GeV}^{-2}$
	$\text{Re}((\bar{c}_F^{(6)})_{221}^{(0E)})$	$(17 \pm 19) \times 10^8 \text{ GeV}^{-2}$
	$\text{Im}((\bar{c}_F^{(6)})_{221}^{(0E)})$	$(114 \pm 59) \times 10^7 \text{ GeV}^{-2}$
	$\text{Re}((\bar{c}_F^{(6)})_{222}^{(0E)})$	$(-3 \pm 19) \times 10^8 \text{ GeV}^{-2}$
	$\text{Im}((\bar{c}_F^{(6)})_{222}^{(0E)})$	$(37 \pm 40) \times 10^7 \text{ GeV}^{-2}$
$d = 8$	$(\bar{c}_F^{(8)})_{220}^{(0E)} - 94(\bar{c}_F^{(8)})_{420}^{(0E)} - 20(\bar{c}_F^{(8)})_{440}^{(0E)}$	$(5 \pm 23) \times 10^{37} \text{ GeV}^{-4}$
	$\text{Re}((\bar{c}_F^{(8)})_{221}^{(0E)}) - 98 \text{Re}((\bar{c}_F^{(8)})_{421}^{(0E)}) + 48 \text{Re}((\bar{c}_F^{(8)})_{441}^{(0E)})$	$(11 \pm 15) \times 10^{36} \text{ GeV}^{-4}$
	$\text{Im}((\bar{c}_F^{(8)})_{221}^{(0E)}) - 98 \text{Im}((\bar{c}_F^{(8)})_{421}^{(0E)}) + 48 \text{Im}((\bar{c}_F^{(8)})_{441}^{(0E)})$	$(39 \pm 15) \times 10^{36} \text{ GeV}^{-4}$
	$\text{Re}((\bar{c}_F^{(8)})_{221}^{(0E)}) - 92 \text{Re}((\bar{c}_F^{(8)})_{421}^{(0E)}) - 11 \text{Re}((\bar{c}_F^{(8)})_{441}^{(0E)})$	$(58 \pm 55) \times 10^{35} \text{ GeV}^{-4}$
	$\text{Im}((\bar{c}_F^{(8)})_{221}^{(0E)}) - 92 \text{Im}((\bar{c}_F^{(8)})_{421}^{(0E)}) - 11 \text{Im}((\bar{c}_F^{(8)})_{441}^{(0E)})$	$(7 \pm 55) \times 10^{35} \text{ GeV}^{-4}$
	$\text{Re}((\bar{c}_F^{(8)})_{222}^{(0E)}) - 96 \text{Re}((\bar{c}_F^{(8)})_{422}^{(0E)}) + 3 \text{Re}((\bar{c}_F^{(8)})_{442}^{(0E)})$	$(66 \pm 29) \times 10^{35} \text{ GeV}^{-4}$
	$\text{Im}((\bar{c}_F^{(8)})_{222}^{(0E)}) - 96 \text{Im}((\bar{c}_F^{(8)})_{422}^{(0E)}) + 3 \text{Im}((\bar{c}_F^{(8)})_{442}^{(0E)})$	$(-26 \pm 28) \times 10^{35} \text{ GeV}^{-4}$
	$\text{Re}((\bar{c}_F^{(8)})_{222}^{(0E)}) - 94 \text{Re}((\bar{c}_F^{(8)})_{422}^{(0E)}) + 49 \text{Re}((\bar{c}_F^{(8)})_{442}^{(0E)})$	$(-8 \pm 24) \times 10^{35} \text{ GeV}^{-4}$
	$\text{Im}((\bar{c}_F^{(8)})_{222}^{(0E)}) - 94 \text{Im}((\bar{c}_F^{(8)})_{422}^{(0E)}) + 49 \text{Im}((\bar{c}_F^{(8)})_{442}^{(0E)})$	$(-25 \pm 25) \times 10^{35} \text{ GeV}^{-4}$
	$\text{Re}((\bar{c}_F^{(8)})_{443}^{(0E)})$	$(-11 \pm 15) \times 10^{33} \text{ GeV}^{-4}$
	$\text{Im}((\bar{c}_F^{(8)})_{443}^{(0E)})$	$(-89 \pm 53) \times 10^{32} \text{ GeV}^{-4}$
	$\text{Re}((\bar{c}_F^{(8)})_{444}^{(0E)})$	$(-5 \pm 29) \times 10^{33} \text{ GeV}^{-4}$
$\text{Re}((\bar{c}_F^{(8)})_{444}^{(0E)})$	$(-10 \pm 28) \times 10^{32} \text{ GeV}^{-4}$	

TABLE II: Measurements of coefficients for Lorentz violation with 1σ errors.

- [2] V.A. Kostelecký and S. Samuel, Phys. Rev. D **39**, 683 (1989); V.A. Kostelecký and R. Potting, Nucl. Phys. B **359**, 545 (1991).
- [3] V.A. Kostelecký and M. Mewes, Phys. Rev. D **80**, 015020 (2009).
- [4] P.L. Stanwix *et al.*, Phys. Rev. D **74**, 081101 (2006).
- [5] M.A. Hohensee *et al.*, Phys. Rev. D **82**, 076001 (2010).
- [6] J. Lipa *et al.*, Phys. Rev. Lett. **90**, 060403 (2003); P. Wolf *et al.*, Gen. Rel. Grav. **36**, 2352 (2004); P. Wolf *et al.*, Phys. Rev. D **70**, 051902 (2004); P.L. Stanwix *et al.*, Phys. Rev. Lett. **95**, 040404 (2005); P.L. Stanwix *et al.*, Phys. Rev. D **74**, 081101 (2006).
- [7] H. Müller *et al.*, Phys. Rev. Lett. **91**, 020401 (2003); S. Herrmann *et al.*, Phys. Rev. Lett. **95**, 150401 (2005); P. Antonini *et al.*, Phys. Rev. A **71**, 050101 (2005); **72**, 066102 (2005); M.E. Tobar, P. Wolf, and P.L. Stanwix, Phys. Rev. A **72**, 066101 (2005); S. Herrmann *et al.*, Phys. Rev. D **80**, 105011 (2009); Ch. Eisele, A.Yu. Nevsky, and S. Schiller, Phys. Rev. Lett. **103**, 090401 (2009).
- [8] H. Müller *et al.*, Phys. Rev. D **67**, 056006 (2003); H. Müller *et al.*, Phys. Rev. D **68**, 116006 (2003); M.E. Tobar *et al.*, Phys. Rev. D **71**, 025004 (2005); H. Müller, Phys. Rev. D **71**, 045004 (2005); H. Müller *et al.*, Phys. Rev. Lett. **99**, 050401 (2007); M. Mewes, Phys. Rev. D **78**, 096008 (2008); M.E. Tobar *et al.*, Phys. Rev. D **80**, 125024 (2009).
- [9] A.A. Michelson and E.W. Morley, Am. J. Sci. **34**, 333 (1887); Phil. Mag. **24**, 449 (1887).
- [10] D. Colladay and V.A. Kostelecký, Phys. Rev. D **55**, 6760 (1997); **58**, 116002 (1998).
- [11] V.A. Kostelecký, Phys. Rev. D **69**, 105009 (2004).
- [12] S.M. Carroll, G.B. Field, and R. Jackiw, Phys. Rev. D **41**, 1231 (1990); V.A. Kostelecký and M. Mewes, Phys. Rev. Lett. **87**, 251304 (2001); **97**, 140401 (2006); **99**, 011601 (2007); Q. Exirifard, arXiv:1010.2054.
- [13] V.A. Kostelecký and M. Mewes, Ap. J. Lett. **689**, L1 (2008).
- [14] V. Vasileiou, arXiv:1008.2913.
- [15] V.A. Kostelecký and M. Mewes, Phys. Rev. D **66**, 056005 (2002).
- [16] M. Tobar and A. Mann, IEEE Trans. on MTT **39**, 2077

(1991); M. Tobar *et al.*, Lect. Notes Phys. **702**, 416 (2006).